Advanced Composite Materials
Publication details, including instructions for authors and subscription information:
http://www.tandfonline.com/loi/tacm20

Stress and Cure Sensing of Single-Shape Memory Alloy (SMA) Fiber/Epoxy Composites using Electro-micromechanical Technique

Joung-Man Park [a], Pyung-Gee Kim [b], Jung-Hoon Jang [c], Zuo-Jia Wang [d], Ga-Young Gu [e], Joel Renaud N. Gnidakoung [f] & K. Lawrence DeVries [g]

[a] School of Materials Science and Engineering, Engineering Research Institute, Gyeongsang National University, Jinju 660-701, Korea, Department of Mechanical Engineering, The University of Utah, Salt Lake City, Utah 84112, USA;, Email: jmpark@gnu.ac.kr

[b] School of Materials Science and Engineering, Engineering Research Institute, Gyeongsang National University, Jinju 660-701, Korea

[c] School of Materials Science and Engineering, Engineering Research Institute, Gyeongsang National University, Jinju 660-701, Korea

[d] School of Materials Science and Engineering, Engineering Research Institute, Gyeongsang National University, Jinju 660-701, Korea

[e] School of Materials Science and Engineering, Engineering Research Institute, Gyeongsang National University, Jinju 660-701, Korea

[f] School of Materials Science and Engineering, Engineering Research Institute, Gyeongsang National University, Jinju 660-701, Korea

[g] Department of Mechanical Engineering, The University of Utah, Salt Lake City, Utah 84112, USA

Version of record first published: 02 Apr 2012.

VSP

Advanced Composite Materials 19 (2010) 139–155

ADVANCED COMPOSITE MATERIALS
brill.nl/acm

Stress and Cure Sensing of Single-Shape Memory Alloy (SMA) Fiber/Epoxy Composites using Electro-micromechanical Technique

Joung-Man Park [a,b,*], **Pyung-Gee Kim** [a], **Jung-Hoon Jang** [a], **Zuo-Jia Wang** [a], **Ga-Young Gu** [a], **Joel Renaud N. Gnidakoung** [a], **K. Lawrence DeVries** [b]

[a] School of Materials Science and Engineering, Engineering Research Institute, Gyeongsang National University, Jinju 660-701, Korea

[b] Department of Mechanical Engineering, The University of Utah, Salt Lake City, Utah 84112, USA

Received 4 December 2008; accepted 13 April 2009

Abstract

SMA (shape memory alloy) is well known to change the microstructure from martensite to austenite with either temperature or stress. Stress and temperature response were investigated for SMA fiber/epoxy composites using an electro-micromechanical technique during curing. SMA fiber can be used in practical applications, including stress or cure-monitoring sensors, due to its inherent shape recovery properties, i.e., it exhibits a shape memory effect (SME) when subjected to applied stress or temperature. Superelasticity was observed for SMA fiber/epoxy composites under cyclic stress–strain curve. Under a certain stress, the original modulus was reduced steeply but then recovered under further stress. A sudden transitional change in electrical resistance was also observed around 87°C with an increase of temperature. Under cyclic loading the stress was suddenly leveled-off with a certain stress, which resulted in a different stress hysteresis repeatedly with two differing matrices and surface treatment. In SMA fiber/epoxy composites, residual stress of single-SMA fiber with and without embedding epoxy matrix exhibited the incomplete and complete recovery, respectively, during the curing process. Interfacial effect between SMA fiber and matrix can be important factor for practical applications including feasible sensing and actuator.

Keywords

Interfacial sensing, superelasticity, electro-micromechanical technique, nondestructive evaluation

1. Introduction

Sensing can usually be carried out by embedding or attaching sensors, which raise cost, reduce durability and degrade the composite's performance. Using electrical resistivity measurement, a new evaluation technique of interfacial properties as well

* To whom correspondence should be addressed. E-mail: jmpark@gnu.ac.kr
Edited by the KSCM

 DOI:10.1163/092430409X12530067339361

as curing characteristics and the residual stress were investigated recently for conductive fiber reinforced self-sensing composites [1–3]. In particular, shape memory alloy (SMA) fiber exhibits certain characteristic properties, including martensite phase transformation, superelastic response and shape memory effect (SME). Polymer matrix composites with functional properties including actuation, damping, and damage recovery have been studied by combining SMA fiber and polymer matrix. Furthermore, conductive SMA fiber reinforced composites were subjected to changing temperature and applied load, which could be studied and their potential explored for use as a new feasible temperature or self-strain sensor as well as actuator.

Recently, medical sensor and engineering applications as smart materials have been exploited. SMA created a memory property by heating, loading, wave, electrical resistance such that the materials were than able to be used for a variety of applications, such as military, medical, safety devices and robotics. Some of current applications of SMA have been in the field of medicine. Tweezers to remove foreign objects through small incisions were invented by NASA. Anchors with SMA hooks to attach tendons to bone were used for Orel Hershiser's shoulder surgery [4–6].

SMA exhibits a shape memory effect and superelasticity as well as corrosion resistance and high bio-compatibility, which cannot be achieved through the use of conventional metal or alloy composites. The shape memory effect is exhibited when the material is in its martensitic phase and deforms in what appears to be a plastic manner. However, the deformation is completely reversible and the original shape recoverable upon heating. When it is loaded in the austenitic phase, superelastic behavior can be observed, wherein the SMA can be stretched up to 10% without permanent deformation upon unloading. In addition, there is significant stress hysteresis between the loading and unloading conditions during surperelastic deformation, leading to exceptional damping properties. The characteristic temperature defining martensitic and austenitic phases is dependent upon SMA composition and heat treatment history [7].

Recently, an electro-micromechanical technique has been studied economically as a new nondestructive evaluation (NDE) method for monitoring of strain and microfailure sensing, curing characteristics, and interfacial properties because conductive fiber can act as a sensor in itself as well as reinforcing fiber [8, 9]. In additions, electrical and mechanical properties of polymer nanocomposites were recently investigated to develop smart materials and to establish fracture or microfailure predicting technique by measuring a change in the electrical resistance under applied loading in conductive composites. Electrical quantities are measured to obtain valuable information on the amount, distribution and orientation of various reinforcing nanomaterials [10–12]. In this work, during curing or under cyclic loading, the electrical resistance in SMA fiber/epoxy composites was evaluated for interfacial properties and nondestructive behaviors depending on the different matrix modulus and temperature.

Table 1.
Structural formulae of DGEBA and Jeffamine

Material	Structural formula
DGEBA	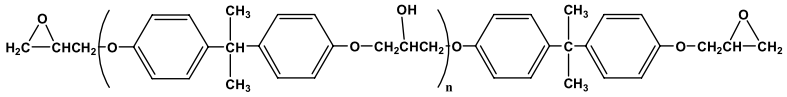
Jeffamine	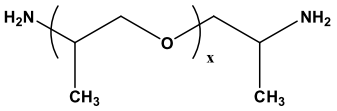

2. Experimental

2.1. Materials

Shape memory alloy (SMA) fiber (40 μm, Furukawa Techno materials Co. Ltd., Japan) was used as conductive reinforcing fiber. Testing specimens were prepared with epoxy resin (YD-128, Kukdo Chemical Co., Korea). Epoxy resin is based on diglycidyl ether of bisphenol-A (DGEBA). Polyoxypropylene diamine (Jeffamine D-400 and D-2000, Huntzman Petrochemical Co.) was used as a curing agent. Table 1 shows structural formulae of DGEBA and Jeffamine. The flexibility of specimens was controlled by adjusting the relative proportion of D-400 *versus* D-2000. Sodium dichromate solution [sodium dichromate ($Na_2Cr_2O_7$), sulfuric acid (H_2SO_4) and double distilled water (H_2O)] of reagent grade was used for the etching of SMA fiber surface. Amino-silane coupling agent, 3-aminopropyl trimethoxysilane (No. 28,177-8, Aldrich Chemical Co.), was also used for the surface treatment on SMA fiber.

2.2. Methodologies

2.2.1. Fiber Surface Treatment of SMA Fiber

SMA fiber was etched in acidified sodium dichromate solution at about 80°C for 20 min. The etched fiber was washed out in distilled water several times until the neutral pH condition was reached and then the fiber was dried at 80°C in an oven. The etched SMA fibers in acidified sodium dichromate solution were treated with amino-silane coupling agent by dipping them into 0.5 wt% silane aqueous solution for one minute at room temperature and then putting them into the oven at 50°C for 4 h.

2.2.2. Preparation of Testing Specimens

Figure 1 shows the schematic illustration of three types of tested specimens for: (a) single-fiber tensile test; (b) temperature of single fiber under electro-micromechanical test; and (c) cure monitoring under electro-micromechanical test. In the single-fiber tensile test case, SMA fiber was fixed in a paper frame using Scotch tape and epoxy adhesive at gauge length of 20 mm. Tensile strength, strain

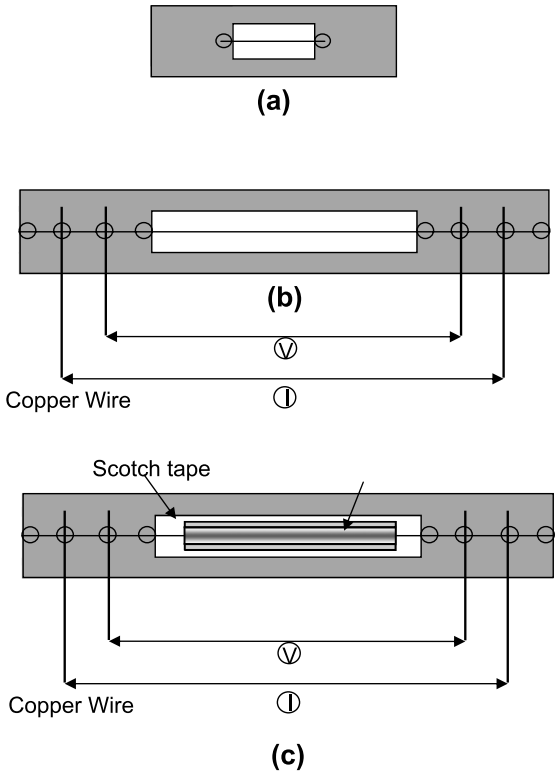

Figure 1. Schematic illustration of three-type testing specimens for: (a) single-fiber tensile test; (b) electro-micromechanical test of single fiber; and (c) electro-micromechanical test/cure monitoring.

and modulus of the SMA fiber were obtained using ten specimens for statistically-meaningful values. Figure 1(b and c) exhibit the testing specimens for electro-micromechanical test or curing. SMA fiber was fixed in a paper frame using Scotch tape and epoxy adhesive at gauge length of 60 mm, and then SMA fiber was embedded in epoxy resin with various conditions, i.e., with or without epoxy matrix, untreated or treated SMA fiber surface, and the ductility of epoxy matrix was explored. SMA fiber/epoxy composites monitored the electrical resistivity during the curing process and then the characteristic change in the electrical properties and nondestructive behavior under cyclic loading was evaluated.

2.2.3. Electrical Resistance Measurement

Figure 2 shows the experimental systems for the measurement of (a) electrical resistivity under cyclic loading; and (b) electrical resistivity with temperature during curing. While curing was in progress and with applied cyclic loading, the electrical resistivity was measured using a digital multimeter (HP34401A). For cure monitoring, the curing cycle was set up as 3 steps that were composed of a precuring step for 2 h at 80°C, the postcuring step for 2 h at 120°C, and the slow cooling down step to room temperature. The cyclic loading test was performed using the mini-

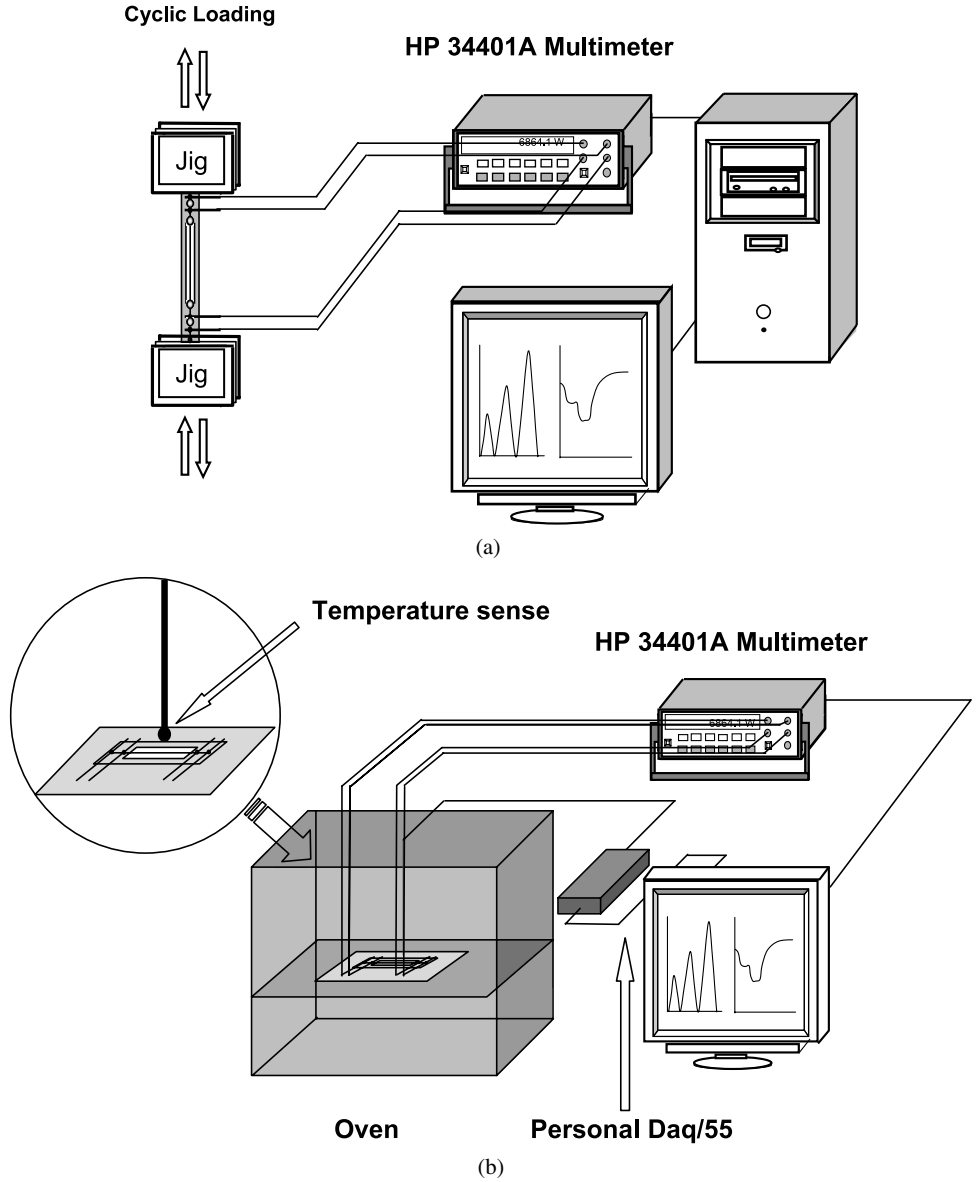

Figure 2. Experimental systems for the measurement of: (a) electrical resistivity with cyclic loading test; and (b) electrical resistivity with temperature or curing.

UTM (H1KS, Hounsfield Equipment Ltd., UK) attached with a multimeter. Testing speed and load cell used were 0.5 mm/min and 100 N, respectively. After a testing specimen was fixed into the mini-UTM grip, nanocomposites and multimeter were connected electrically using thin copper wires. While 5 cyclic loadings were applied, the electrical resistivity of SMA fiber was measured simultaneously with stress–strain change until the same and changeable maximum load was reached.

Electrical resistivity was obtained from the measured electrical resistance, cross-sectional area of the conductive fiber, A, and electrical contact length, L_{ec} of the testing fiber connecting to copper wire. The relationship between electrical resistivity, ρ and resistance R is as follows [13],

$$\rho = \left(\frac{A}{L_{ec}}\right) \times R. \tag{1}$$

3. Results and Discussion

3.1. Shape Memory Effect of SMA Fiber by Applied Load and Temperature

Figure 3 shows the schematic plot of the change of crystal structure during shape memory transformation. The shape memory effect was related to the temperature, loading and the change in crystal shape. SMA fiber has been known to be not plastic but more elastic in nature. When heated, a shape memory alloy transforms to the austenite phase having a body centered cubic (BCC) microstructure. Upon cooling, the SMA transforms to a martensite phase with a less rigid monoclinic structure, which permits the coexistence of multiple variants of martensite.

The transformation involves two processes — the Bain strain and the lattice-invariant shear. The Bain strain incorporates small movements of atoms needed to produce the new crystal structure of martensite. The lattice-invariant shear mechanism accommodates the different shape of the new martensite within the transformed austenite. The uniqueness of shape memory lies in the fact that the lattice-invariant shear step of this transformation occurs almost solely by twinning [14, 15]. Twinning forces the BCC shape into a monoclinic phase with no volumetric change

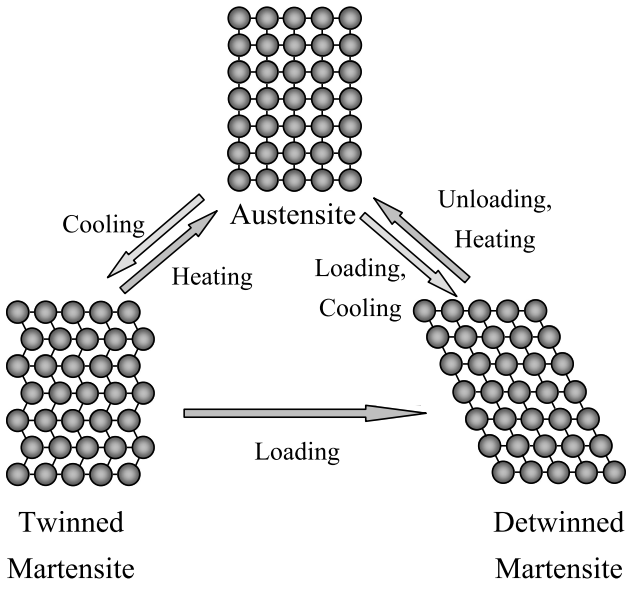

Figure 3. Schematic change of crystal during shape memory behavior.

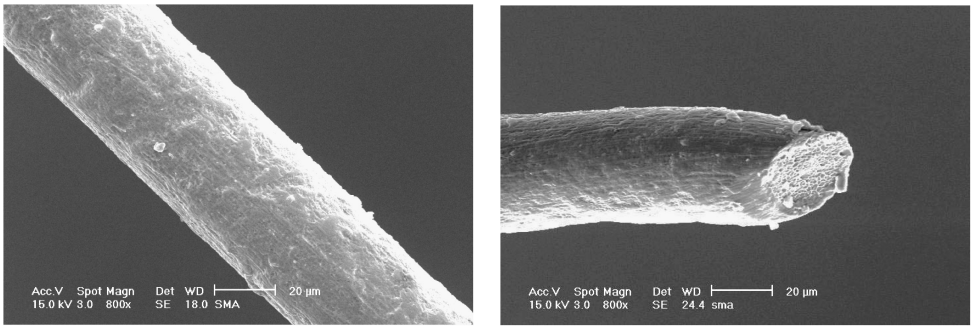

Figure 4. Morphology of the SMA fiber for: (a) fiber surface; (b) microfailure mode under tensile.

and no broken bonds. The tilted monoclinic shape forms alternate bands, producing a herringbone effect. When stress is applied to this structure, the alternate bands align in the same direction by a process called 'de-twinning'. When the material is again heated to the austenitic phase, the de-twinned crystal structure transforms back to BCC austenite and regains its original shape.

Applied stress has a significant effect on the transformation characteristics of shape memory alloy [16, 17]. In martensitic transformation, there is a relationship between stress and temperature. A decrease in temperature is equivalent to an increase in stress, both stabilizing martensite. The transformation temperature increases approximately linearly with applied stress.

Figure 4 shows SEM photographs of the SMA fiber for (a) initial fiber surface and (b) catastrophic failure mode after tensile yielding. Figure 4(a) shows uniform fiber diameter and a slightly roughened surface. Figure 4(b) shows that the fiber diameter was rather reduced based on plastic deformation after fracture under tensile, and the fractured surface also exhibited a rough surface with many water-droplet patterns, which resulted in mechanical interlocking with epoxy matrix.

Figure 5 shows the typical stress–strain curve of a single-SMA fiber under tensile stress. The curve was divided into three regions based on the change in crystal shape under applied stress. In region A the crystal shape was twinned martensite, whereas in region B, the super-elasticity behavior resulted in shear stress due to the change in crystal structure from twinned martensite to de-twinned martensite. Finally, crystal shape was de-twinned martensite in C region.

Table 2 shows mechanical properties of SMA fiber during shape memory behavior under applied stress. Young's modulus and elongation of each region were different, respectively, due to different crystal structure. Especially, superelasticity behavior occurred at about 700 MPa and the modulus of region B was really zero due to the shear stress induced by the change of crystal structure.

Figure 6 shows the change in electrical resistivity, $\Delta\rho$, with temperature. Electrical resistivity decreased suddenly under the initial condition as temperature increased and then increased steadily from above 87°C transition temperature due to the change in crystal shape with the temperature.

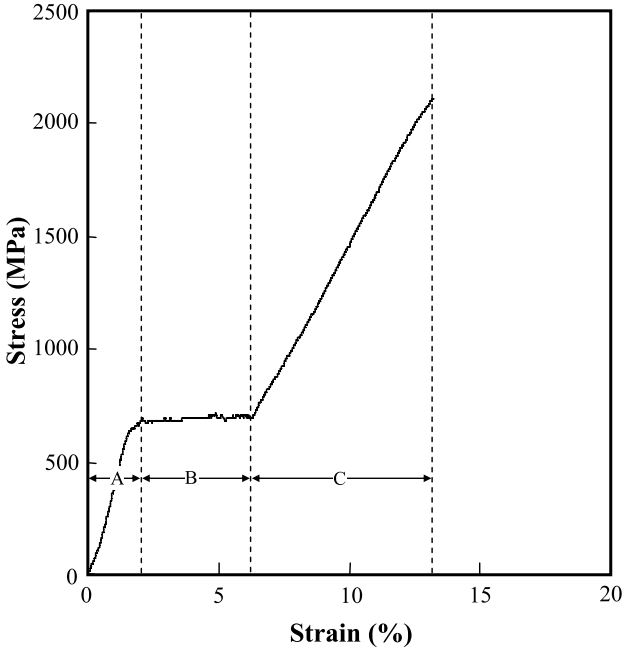

Figure 5. Typical stress–strain curve of single-SMA fiber under tensile stress.

Table 2.
Mechanical properties of SMA fiber during shape memory behavior by applied stress

Region	Stress at super-elasticity (MPa)	Fracture stress (MPa)	Modulus (GPa)	Elongation (%)	Fracture elongation (%)
A	–		42 (3.5)	2.0 (0.2)	
B	722 (14)		0 (0.0)	4.8 (0.4)	
C	–	1916 (152)[a]	21 (1.2)	6.4 (0.9)	12.9 (1.1)

[a] Standard deviation (SD).

3.2. Bare SMA Fiber and SMA Fiber/Epoxy Composites under Cyclic Loading

Figure 7 shows stress–strain curves with cyclic loading test of single-SMA fiber: (a) without epoxy matrix; and (b) with epoxy matrix. Superelasticity behavior exhibited the stress hysteresis under uniform cyclic loading based on the change of internal structure of materials. The strain taking to the maximum strength was much shorter for the epoxy matrix embedded composite since embedded epoxy constrained the SMA fiber. At initial and maximum positions, strain hysteresis also occurred in Fig. 7(a and b). In the bare SMA fiber case, strain hysteresis was more significant than the embedded epoxy matrix case in the initial stage, whereas in epoxy matrix embedded case, stress hysteresis was observed more than without

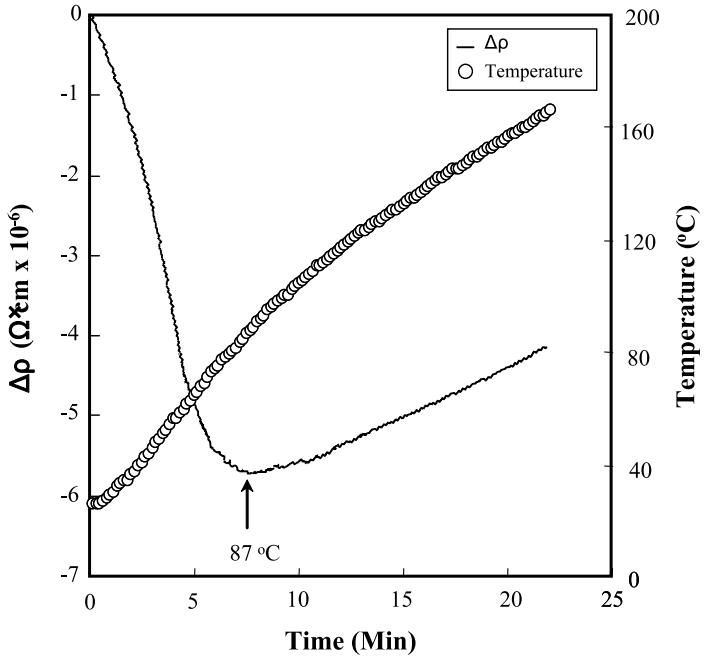

Figure 6. Change in electrical resistivity, $\Delta\rho$ with temperature.

epoxy matrix at the maximum stress region. This is because the slippage could occur consequently at the interface between SMA fiber and epoxy matrix. In addition, the strain increased steadily due to the incomplete recovery and the delay under cyclic loading. The maximum transforming stresses during both tensile and recovery stages were much higher than for the bare SMA fiber cases. It might be because more constraining compressive stress from epoxy matrix could contribute to reduce the transforming stresses.

Figure 8 shows the change in electrical resistivity with cyclic test of single-SMA fiber: (a) without epoxy matrix; and (b) with epoxy matrix. The time taken for five cycles of strain for SMA fiber/epoxy composites was much shorter than for bare SMA fiber. As applied stress and strain increased and decreased repeatedly, electrical resistivity and stress responded with corresponding superelasticity. The stress at superelasticity decreased gradually with uniform cyclic loading.

Figure 9 shows the change in electrical resistivity with loading/unloading test of single-SMA fiber: (a) without epoxy matrix; and (b) with epoxy matrix. Two figures showed a completely different pattern of the change in electrical resistivity. The change in electrical resistivity was significantly dependent upon the existence of epoxy matrix. At the same test speed, strains were different due to the epoxy matrix. In other words, the change in electrical resistivity being consistent with the change in crystal shape is related to the interfacial property between SMA fiber and epoxy matrix.

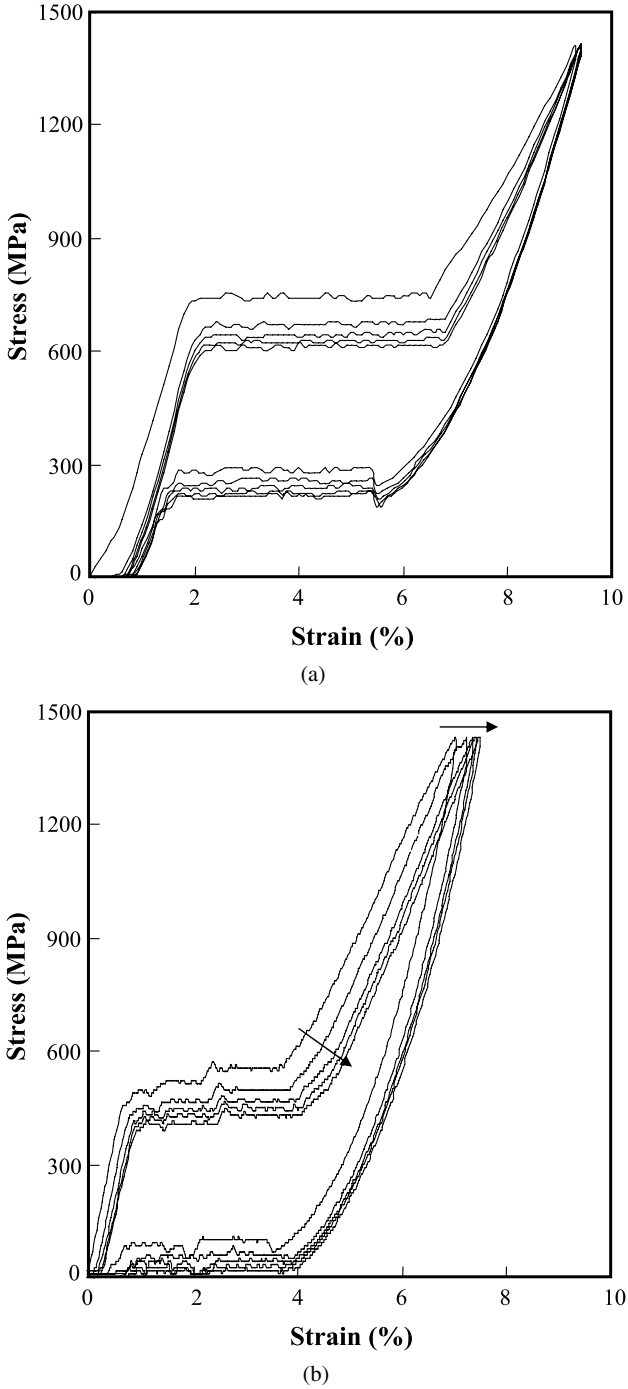

Figure 7. Stress–strain curves with cyclic loading test of single-SMA fiber: (a) without epoxy matrix; and (b) with epoxy matrix.

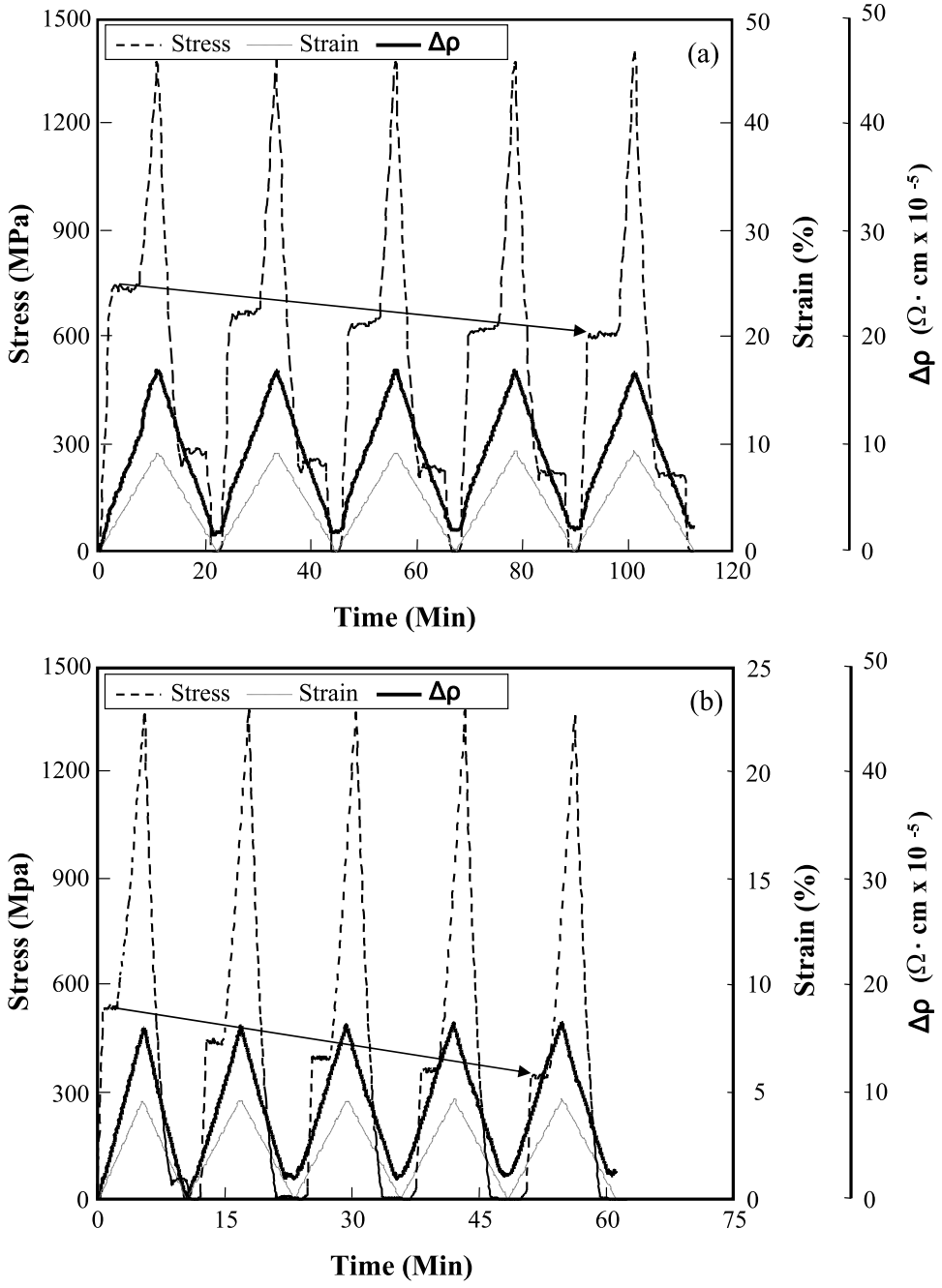

Figure 8. Change in electrical resistivity with cyclic test of single-SMA fiber: (a) without epoxy matrix; and (b) with epoxy matrix.

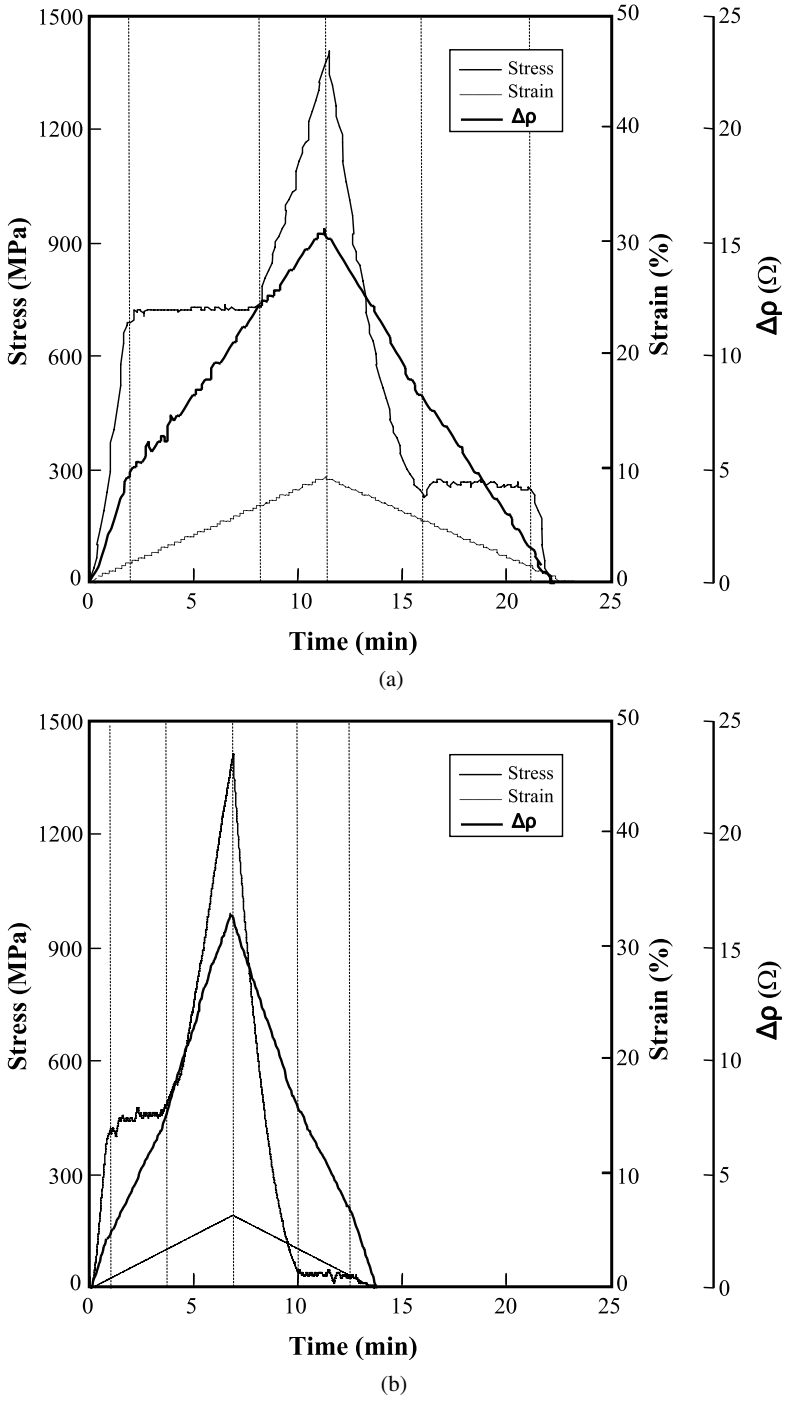

Figure 9. Change in electrical resistivity with loading/unloading test of single-SMA fiber: (a) without epoxy matrix; and (b) with epoxy matrix.

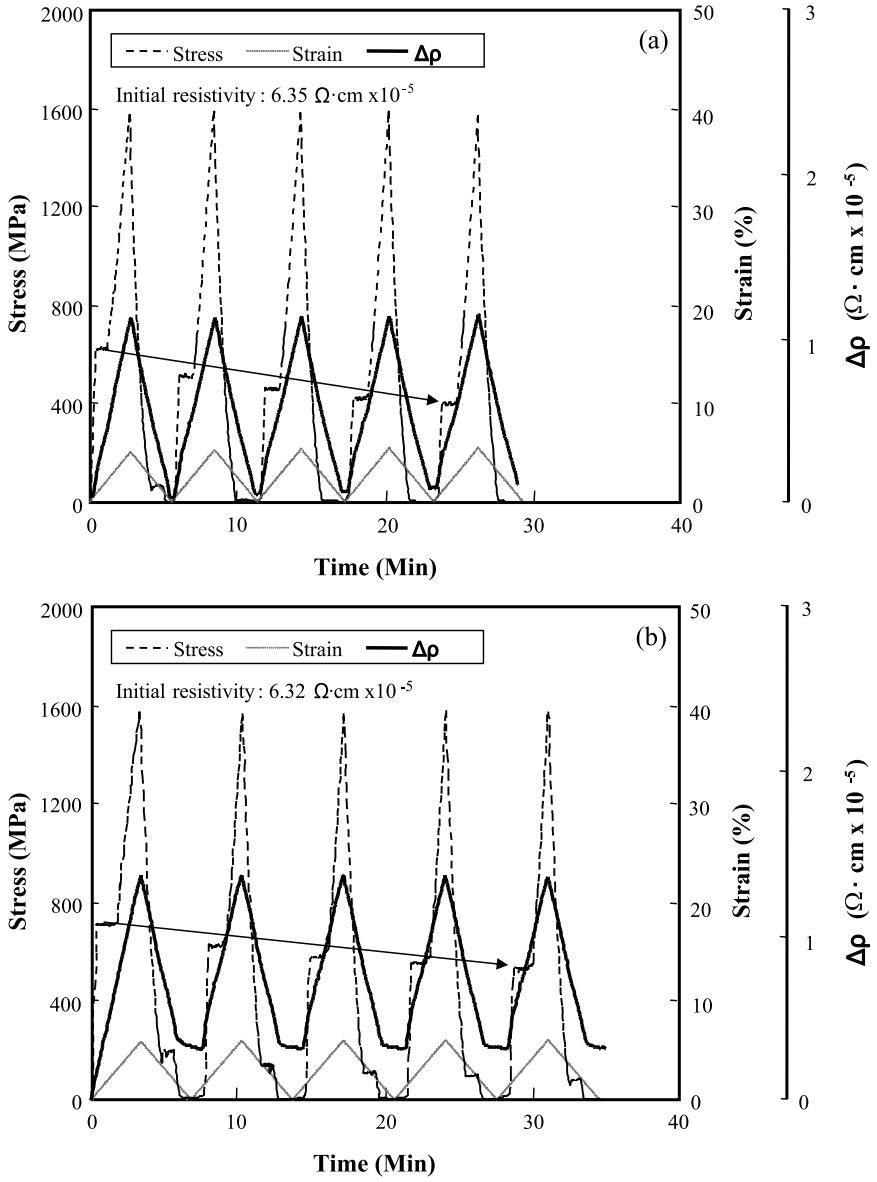

Figure 10. Change in electrical resistivity with cyclic loading test of SMA fiber/epoxy composites with: (a) conventional epoxy matrix; (b) rigid epoxy matrix; and (c) modified surface condition of SMA fiber.

Figure 10 shows the change in electrical resistivity with cyclic loading test of single-SMA fiber/epoxy composites with: (a) conventional epoxy matrix; (b) rigid epoxy matrix; and (c) modified surface condition of SMA fiber. The change in the electrical resistivity shows different interfacial bonding between fiber and matrix. In the rigid epoxy matrix case, electrical resistivity does not return to its initial

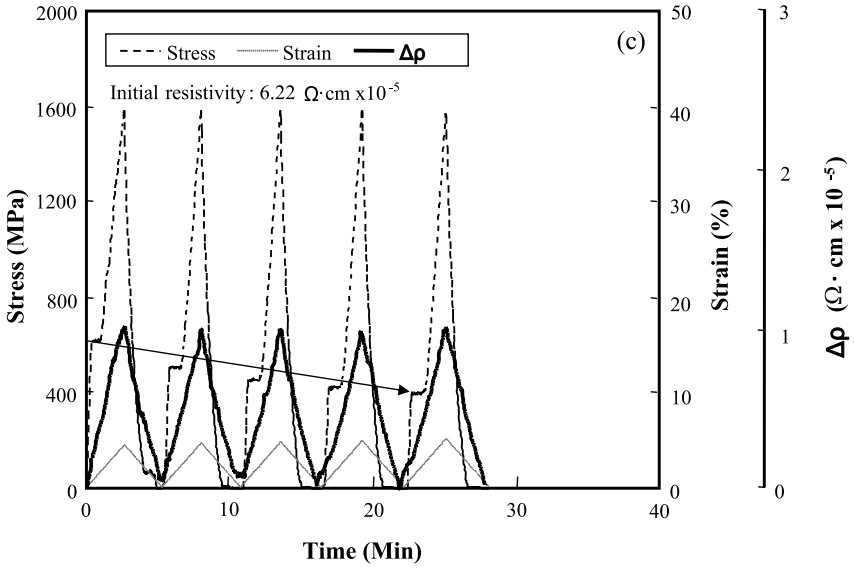

Figure 10. (Continued.)

Table 3.
Comparison of mechanical properties at first cycle loading/unloading with various conditions

Conditions	Modulus at first region (GPa)	Superelasticity stress (MPa)	Strain of max. stress (%)
Untreated SMA fiber/conventional epoxy	115	615	4.7
Untreated SMA fiber/rigid epoxy	240	717	5.5
Surface treated SMA fiber/conventional epoxy	120	618	4.6

state due to the slippage between fiber and matrix. In modified surface condition of SMA fiber, electrical resistivity does return to the initial state completely because of increased interfacial adhesion. Table 3 shows the comparison of mechanical properties at the first loading/unloading cycle with various conditions. In the rigid epoxy case, modulus and superelasticity stress at the first region was higher than others whereas the strain at the maximum stress was larger than others due to the slippage between fiber and matrix. The surface treated SMA fiber exhibited slightly higher modulus at the first region.

3.3. The Change in Electrical Resistivity During Curing

Figure 11 shows the change in electrical resistivity of SMA fiber itself with temperature change: (a) temperature increase and decrease, gradually; and (b) curing temperature profile. Figure 11(a) shows the change in temperature increased from 30°C to 150°C and then decreased to 30°C slowly. Electrical resistivity corre-

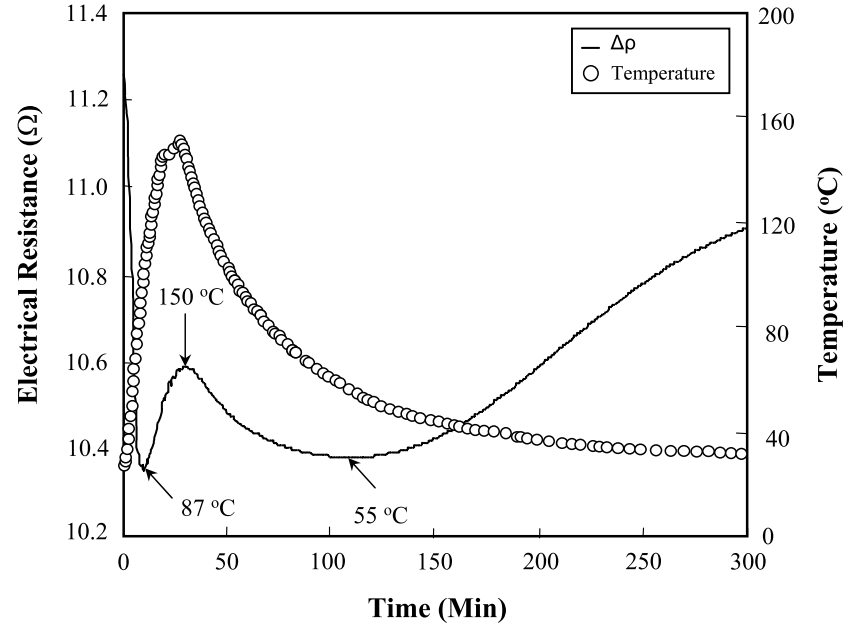

(a)

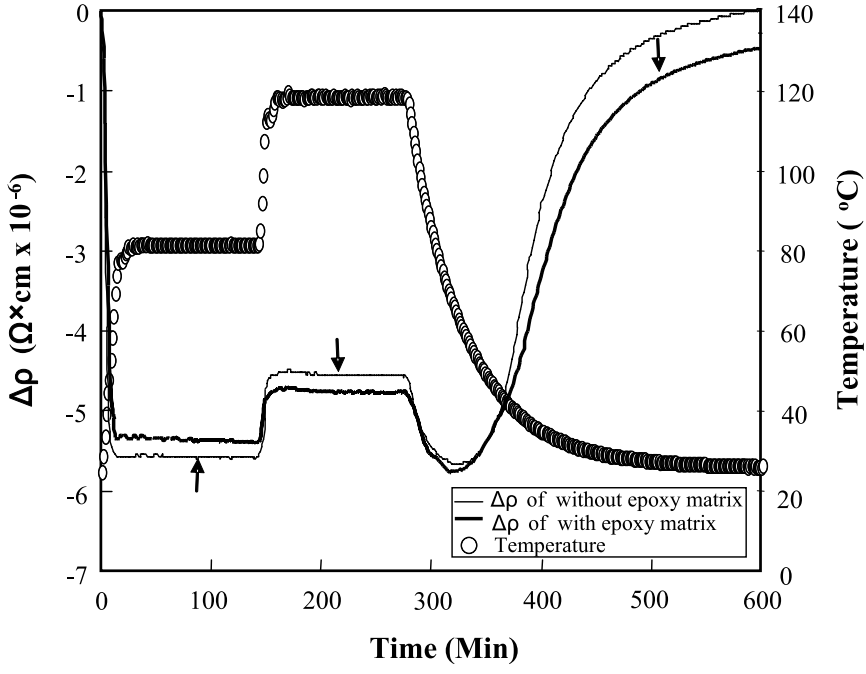

(b)

Figure 11. Change in electrical resistivity of SMA fiber itself with temperature change: (a) temperature increase and decrease, gradually; and (b) curing temperature profile.

sponded closely to the temperature change. The change in electrical resistivity exhibited three transition points at 87°C, 150°C and 55°C, respectively. Especially the cause of the change in electrical resistivity at 87°C and 55°C were due to the change in crystal shape, from martensite/or austenite to austenite/or martensite. Although 87°C and 55°C seem to be rather far apart, 55°C could mark the start of a gradual change and the reverse transition occurring from 87°C in the same way. Figure 11(b) shows the change in electrical resistivity with epoxy curing temperature for bare SMA fiber and SMA fiber embedded with epoxy. Electrical resistivity responded well with temperature change for both cases. In the epoxy matrix embedded case, the electrical resistivity did not return to the original point after temperature decreased to room temperature, whereas bare SMA fiber returned to the original point.

4. Conclusions

The change in electrical resistivity of SMA fiber/epoxy composites with shape memory behavior of SMA fiber was investigated by the electrical resistivity measurement under micromechanical tests. Shape memory behavior was related to the temperature loading due to the change in crystal shape. SMA fiber was not plastic but visibly elastic. The stress–strain curve of single-SMA fiber under tensile test was divided into three typical regions based on the change in crystal shape. In the temperature increase case, electrical resistivity decreased dramatically initially up to 87°C, and then increased again due to the change in crystal shape.

Superelasticity behavior exhibited the stress hysteresis under uniform cyclic loading based on the change of internal structure of SMA. Under uniform cyclic loading, the strain up to the maximum strength for epoxy matrix embedded SMA fiber composite was shorter than for the bare SMA fiber case. Just as the applied stress and strain increased and then decreased incrementally, so the electrical resistivity and stress also responded correspondingly. Especially, the change in electrical resistivity was different with the change in crystal shape as applied stress and strain increased. In other words, the change in electrical resistivity was consistent with the change in crystal shape. Electrical resistivity responded well to temperature as well. The change in electrical resistivity showed three distinct transition points at 87°C, 150°C and 55°C, respectively. Especially the changes in electrical resistivity at 87°C and 55°C were due to the change in crystal shape. As far as the curing process and cyclic loading are concerned, the interfacial effect between SMA fiber and matrix will be an important parameter for practical applications including feasible sensing and actuator.

Acknowledgements

Zuo-Jia Wang is grateful to the second stage of BK21 program for supporting a fellowship.

References

1. D. M. Bontea, D. D. L. Chung and G. C. Lee, Damage in carbon fiber-reinforced concrete, monitored by electrical resistance measurement, *Cement Concr. Res.* **30**, 651–659 (2000).
2. K. Yue and C. Bathias, Smart NDT using electrical resistance method for delamination monitoring in CFRP, in: *Proc. ICCM-12*, Paris, France, pp. 767–776 (1999).
3. B. Frakhanel, E. Muller, T. Frakhanel and W. Siegel, Conductive SiC-fibre reinforced composites as a model of 'smart composites', *J. Europ. Ceram. Soc*. **18**, 1821–1825 (1998).
4. A. V. Srinivasan and D. M. McFarland, *Smart Structure: Analysis and Design*. Cambridge University Press, Cambridge, UK (2001).
5. D. E. Hongson, *Using Shape Memory Alloys*. Cupertino, California, USA (1995).
6. N. Nayan, Govind, C. N. Saikrishna, K. V. Ramaiah, S. K. Bhaumik, K. S. Nair and M. C. Mittal, Vacuum induction melting of NiTi shape memory alloys in graphite crucible, *Mater. Sci. Engng. A* **465**, 44–48 (2007).
7. N. A. Smith, G. G. Antoun, A. B. Ellis and W. C. Crone, Improved adhesion between nickel–titanium shape memory alloy and a polymer matrix *via* silane coupling agents, *Composites Part B* **35**, 1307–1312 (2004).
8. X. Wang and D. D. L. Chung, Residual stress in carbon fiber embedded in epoxy, studied by simultaneous measurement of applied stress and electrical resistance, *Compos. Interfaces* **5**, 277–281 (1998).
9. X. Wang and D. D. L. Chung, An electromechanical study of the transverse behavior of carbon polymer–matrix composites, *Compos. Interfaces* **5**, 191–199 (1998).
10. J. M. Park, D. S. Kim, S. J. Kim, P. G. Kim, D. J. Yoon and K. L. DeVries, Inherent sensing and interfacial evaluation of carbon nanofiber and nanotube/epoxy composites using electrical resistance measurement and micromechanical technique, *Composites Part B* **38**, 847–861 (2007).
11. J. M. Park, S. J. Kim, J. H. Jang, Z. Wang, D. J. Yoon, J. W. Kim, G. Hansen and K. L. DeVries, Actuation of electrochemical, electro-magnetic, and electro-active actuators for carbon nanofiber and Ni nanowire reinforced polymer composites, *Composites Part B* **39**, 1161–1169 (2008).
12. J. M. Park, P. G. Kim, J. H. Jang, Z. Wang, W. I. Lee, J. G. Park and K. L. DeVries, Self-sensing and interfacial evaluation of single carbon fiber/carbon nanotube (CNT)-epoxy composites using electro-micromechanical technique and nondestructive acoustic emission, *Composites Part B* **39**, 1170–1182 (2008).
13. J. M. Park, S. I. Lee, K. W. Kim and D. J. Yoon, Interfacial properties of electrodeposited carbon fiber/epoxy composites using electro-micromechanical technique and nondestructive evaluation, *J. Colloid Interf. Sci.* **237**, 80–90 (2001).
14. S. Miyazaki, K. Otsuka and C. M. Wayman, The shape memory mechanism associated with the Martensitic Transformation in Ti-Ni alloys-II. Variant coalescence and shape recovery, *Acta Metallurgica* **37**, 1885–1890 (1989).
15. J. B. Berman and S. R. White, Theoretical modeling of residual and transformational stresses in SMA composites, *Smart Mater. Struct*. **5**, 731–743 (1996).
16. H. U. Schuerch, Certain physical properties and applications of Nitinol, *NASA CR-1232*, November (1968).
17. Z. G. Wei and S. Miyazaki, Review shape-memory materials and hybrid composites for smart systems, *J. Mater. Sci*. **33**, 3743–3762 (1998).